

# Long range chromomagnetic fields at high temperature

S. Antropov <sup>a</sup>, M. Bordag <sup>b,\*</sup>, V. Demchik <sup>a,†</sup> and V. Skalozub <sup>a,‡</sup>

<sup>a</sup> *Dnipropetrovsk National University, 49010 Dnipropetrovsk, Ukraine*

<sup>b</sup> *University of Leipzig, Institute for Theoretical Physics,  
Postfach 100 920, 04009 Leipzig, Germany*

May 3, 2022

## Abstract

The magnetic mass of neutral gluons in Abelian chromomagnetic field at high temperature is calculated in  $SU(2)$  gluodynamics. It is noted that such type fields are spontaneously generated at high temperature. The mass is computed either from the Schwinger-Dyson equation accounting for the one-loop polarization tensor or in Monte-Carlo simulations on a lattice. In latter case, an average magnetic flux penetrating a plaquette is measured for a number of lattices. Both calculations are in agreement with each other and result in zero magnetic mass. Some applications of the results obtained are discussed.

## 1 Introduction

Investigation of deconfinement phase of QCD is a topic of actual interest in modern high energy physics. For instance, it is related to confinement models involving monopole condensation in the dual superconductor scenario. Further it is discussed as lowering the phase transition temperature [1]. It is also of interest for the QCD phase diagram, for quark-gluon plasma and related topics like the state of the early universe.

As it was discovered recently, in the non-Abelian gauge theories at high temperature a spontaneous vacuum magnetization happens. This has been determined either by analytic quantum field theory methods [2], [3], [5], [4] or in

---

\*E-mail: Michael.Bordag@itp.uni-leipzig.de

†E-mail: vadimdi@yahoo.com

‡E-mail: skalozubv@daad-alumni.de

lattice simulations [6]. This phenomenon is analogous to the spontaneous creation of Abelian chromomagnetic field  $B = const$  discovered at zero temperature  $T = 0$  by Savvidy [7]. However, as it is well known, this vacuum is unstable. The instability follows from the tachyon mode  $p_0^2 = p_{||}^2 - gB$  presenting in the gluon spectrum,

$$p_0^2 = p_{||}^2 + (2n + 1)gB, \quad n = -1, 0, 1, \dots, \quad (1)$$

where  $p_{||}$  is a momentum component along the field,  $B$  is field strength,  $g$  is gauge coupling constant. The evolution of the instability is resulted in a condensate. Thus, at  $T = 0$  the Abelian constant chromomagnetic field is completely screened. Then interesting question arises: whether high temperature can suppress the instability inherent to such a state?

As it is occurred, the situation changes at finite temperature  $T \neq 0$  and the spectrum stabilization happens due to either a gluon magnetic mass [4] or so-called  $A_0$ -condensate which is proportional to the Polyakov loop [8]. These are the extensions of the Savvidy model to the finite temperature case. In this way a possibility of spontaneous generation of the strong temperature-dependent and stable color magnetic fields of order  $gB \sim g^4 T^2$  is realized. Further investigations of quarks and gluons at this background are of interest if the generated classical fields are long range ones. In fact, this means that the field scale is larger than Compton's wave length of a particle.

The most essential field characteristics at finite temperature are the electric (Debye) and magnetic masses responsible for screening of long range color electric and magnetic fields, respectively. Debye's mass of gluons in the field presence has been calculated already (see, for instance, [10], [11]). It was derived as some function of temperature and field strength. As concerns the magnetic mass, it requires an additional consideration that is the topic of the present investigation. The point is that in the field presence it is natural to divide gluons in two types - the charged and the neutral gluons, - which have different magnetic masses at high temperatures. For the former fields, the nonzero magnetic mass has been determined in one-loop order [4]. For the latter one this problem is not solved finally. The zero value has been obtained in one-loop approximation in Refs.[9], [10]. However, the role of higher order corrections remains not investigated, yet. Just this point need to be studied in more details. In sections 2 we calculate the neutral gluon magnetic mass by means of quantum field theory methods. In section 3 the magnetic mass of Abelian chromomagnetic field is computed by using Monte-Carlo simulations. In both computations a zero magnetic mass is obtained. This, in particular, means that the spontaneously created at high temperature Abelian chromomagnetic fields are long range similarly to the case of usual  $U(1)$  magnetic field. The discussion and possible applications are given in section 4.

## 2 Magnetic mass of neutral gluons

In this section we calculate the magnetic mass of neutral gluons by using analytic quantum field theory methods. In this approach, the gluon magnetic mass can be determined in the imaginary time formalism through the polarization tensor (PT),

$$m_{magn.}^2(s) = \langle s | \Pi(k, B, T) | s \rangle_{k_4=0, k^2 \rightarrow 0} . \quad (2)$$

Here,  $k_4 = 2\pi NT$ ,  $N = 0, \pm 1, \pm 2, \dots$  is a Matsubara frequency,  $k^2$  is a momentum squared. The mean value is calculated in the two states of polarization (denoted as  $s = 1$  and  $s = 2$  [13], [10]) transverse to the gluon momentum  $k_\mu$ .

In actual calculation, we consider  $SU(2)$  gluodynamics and assume that the Abelian chromomagnetic field is directed along the third axis in coordinate and internal spaces. In the Landau gauge it is described by the potential

$$A_\mu^a = \delta^{a3}(0, 0, Bx^1, 0), \quad B = const. \quad (3)$$

This is solution to classical field equations without source terms. So, such field can create spontaneously. For chosen field configuration it is convenient to decompose the potential as neutral  $A_\mu = A_\mu^3$  and charged  $W_\mu^\pm = \frac{1}{\sqrt{2}}(A_\mu^1 \pm A_\mu^2)$  gluons, where  $a = 1, 2, 3$  is a color index. Just for the latter gluons the tree-level spectrum is written in Eq.(1).

General strategy of calculation and the particular definitions of quantities to calculate are the same as in Ref.[10]. In the neutral PT case, there are no states unstable in tree approximation. The instability (and related to it the imaginary part of PT) appears because of the tachyon mode propagating inside loops. In tree-approximation, there are two transverse with respect to the gluon momentum  $k_\mu$  states of polarization  $s = 1$  and  $s = 2$  [13], [10]. We introduce the notations:  $l_4 = k_4$  and  $h^2 = l_1^2 + l_2^2$  are transverse with respect to external field ( $B = B_3$ ) momentum components and  $k^2 = h^2 + l_3^2$ ,  $l^2 = l_3^2 + l_4^2$ . To consider the behavior of the static modes  $l_4 = 0$  in perpendicular with respect to the field direction we set  $l_3 = 0$ . Then the magnetic mass of them is defined as the mean values of the PT in the states  $s$  calculated in the limit of  $h^2 \rightarrow 0$ :

$$m_{magn.}^2(s) = \langle s | \Pi(k, B, T) | s \rangle_{k_4=0, h^2 \rightarrow 0} . \quad (4)$$

The neutral PT is calculated in the form given in Eq.(38) of Ref. [10]:

$$\Pi_{\lambda\lambda'}(k) = \sum_{i=1}^{10} \Pi^{(i)}(k, B, T) T_{\lambda\lambda'}^{(i)} , \quad (5)$$

where  $T_{\lambda\lambda'}^{(i)}$  are the structures out of the momentum  $k_\mu$ , medium velocity  $u_\mu$  and  $\delta_{\lambda\lambda'}$  and the form factors  $\Pi^{(i)}(k)$  depend on the external momentum  $k_\mu$  through the variables  $l^2$  and  $h^2$  at zero temperature and  $h^2$ ,  $k_4$  and  $k_3$  at finite temperature.

Within the developed formalism, the polarization tensor becomes the expression of the type

$$\Pi_{\lambda\lambda'}(k) = \int_0^\infty \int_0^\infty ds dt M_{\lambda\lambda'}(p, k) \langle \Theta_T(s, t) \rangle, \quad (6)$$

where in  $M_{\lambda\lambda'}(p, k)$  we collected all factors appearing from the vertexes and from the lines except for that going into  $\Theta_T(s, t)$  (Eq.(59) in Ref. [10]):

$$\begin{aligned} \langle \Theta(s, t) \rangle_T &= \sum_{N=-\infty}^{+\infty} \langle \Theta(s, t) \rangle \exp \left( -\frac{N^2}{4T^2(s+t)} + i \frac{k_4 t N}{(s+t)T} \right) \\ &= \sum_{N=-\infty}^{+\infty} \Theta_T(s, t). \end{aligned} \quad (7)$$

We introduced the notation  $\Theta_T(s, t)$  which is the basic function appearing in all form factors,  $N$  is discrete energy variable. The function  $\langle \Theta(s, t) \rangle$  is given in Eq.(47) of Ref.[10]:

$$\langle \Theta \rangle = \frac{\exp \left[ -k \left( \frac{st}{s+t} \delta^\parallel + \frac{ST}{S+T} \delta^\perp \right) k \right]}{(4\pi)^2 (s+t) \sinh(s+t)} \quad (8)$$

with  $S = \tanh(s)$  and  $T = \tanh(t)$ .

Here and below, as in Ref.[10], for simplicity we set the field strength  $gB = 1$ . That means we measure all quantities in units of  $gB$ . To return to the dimensionfull variables one has to substitute  $s \rightarrow gBs$ , etc.

The factors  $M^{(i)}$  giving contributions to the matrix elements of  $\Pi$  for the infrared limit of interest in Eq.(4) to the states  $s = 1, s = 2$  are [10]:

$$\begin{aligned} M_2 &= 4 \frac{1 - \cosh(q) \cosh(\xi)}{(\sinh(q))^2} - 2 + 8 \cosh(q) \cosh(\xi), \\ M_3 &= -2 \cosh(2q) \frac{\xi \sinh(\xi)}{q \sinh(q)} - 2 + 6 \cosh(\xi) \cosh(q), \\ M_5 &= -2 + 2 \cosh(q) \cosh(\xi), \end{aligned} \quad (9)$$

where  $q = s+t, \xi = s-t = q(2u-1)$  and  $s = qu, t = q(1-u)$ . The contributions to the particular polarization states  $s$  are (Eq.(142) Ref.[10]):

$$\begin{aligned} \langle s=1 | \Pi(k) | s=1 \rangle &= h^2 \Pi_2, \\ \langle s=2 | \Pi(k) | s=2 \rangle &= h^2 (\Pi_3 + \Pi_5). \end{aligned} \quad (10)$$

In this way, these matrix elements are the product of  $h^2$  and expressions which have a finite limit for  $h^2 = 0$ ,

$$\Pi_i = \Pi_i^{(0)} + O(h^2). \quad (11)$$

The quantities  $\Pi_i^{(0)}$  were calculated in [10] numerically. In fact, it is possible to calculate them analytically in terms of simple zeta functions.

From the above expressions (6)-(9), in leading order for  $T \rightarrow \infty$ , which picks just the  $N = 0$ -contribution, we note

$$\Pi_i^{(0)} = \frac{g^2}{(4\pi)^{3/2}} \frac{T}{\sqrt{gB}} \int_0^1 du \int_0^\infty \frac{dq\sqrt{q}}{\sinh(q)} M_i(q, u). \quad (12)$$

In these expressions, the integration over  $u$  can be carried out explicitly,

$$\Pi_i^{(0)} = \frac{g^2}{(4\pi)^{3/2}} \frac{T}{\sqrt{gB}} \int_0^\infty \frac{dq\sqrt{q}}{\sinh(q)} M_i(q) \quad (13)$$

with

$$\begin{aligned} M_2(q) &= -2 - \frac{4}{q} \coth(q) + \frac{4}{\sinh(q)^2} + \frac{4}{q} \sinh(2q), \\ M_3(q) &= -2 - \frac{2}{q^2} \cosh(2q) (-1 + q \coth(q)) + \frac{3}{q} \sinh(2q), \\ M_5(q) &= -2 + \frac{1}{q} \sinh(2q), \end{aligned} \quad (14)$$

and the  $q$ -integrations remain.

These expressions are formally divergent for  $q \rightarrow \infty$ . This divergence results from the tachyonic mode. Here we have to remember that all above formulas are written in Euclidean representation (basically, for technical reasons). In fact, we have to start from the Minkowski space representation which can be reached by an 'Anti'-Wick rotation,  $q \rightarrow qe^{i\pi/2}$ . In the Minkowski space representation the parametric integrals are convergent using the usual ' $i\epsilon$ '-prescription. But then, the contribution from the tachyonic mode in the loop cannot be Wick-rotated since, in momentum space, the corresponding pole is on the 'wrong' side of the imaginary axis of the momentum  $p_0$ . However, it can be 'Anti'-Wick rotated delivering a exponentially fast converging integral. The remaining part can be Wick rotated as usual. In this way, if starting from the Euclidean representation, the tachyonic part must be 'Anti'-Wick rotated twice,  $q \rightarrow qe^{i\pi}$ . The remaining part can be kept as is. The subdivision into tachyonic and remaining parts must be done according to the behavior for  $q \rightarrow \infty$ . There is a freedom left of redistribution power like contributions. It can be used to avoid singularities in  $q = 0$ .

We make the following subdivision into tachyonic parts (parts A),

$$M_2^A = \left[ \frac{4}{q} e^q \right] \sinh(q),$$

$$\begin{aligned}
M_3^A &= \left[ \left( \frac{2(1-q)}{q^2} + \frac{3}{q} \right) e^q - \frac{2}{q^2} \right] \sinh(q), \\
M_5^A &= \left[ \frac{1}{q} e^q \right] \sinh(q),
\end{aligned} \tag{15}$$

and remaining parts (parts B),  $M_i^B = M_i - M_i^A$ .

Being inserted into (13), after the 'Anti'-Wick rotation, the A-parts constitute simple integrals which can be done immediately (for the moment we drop the common prefactors),

$$\begin{aligned}
\Pi_2^{(0),A} &= 4i\sqrt{\pi}, \\
\Pi_3^{(0),A} &= 5i\sqrt{\pi}, \\
\Pi_5^{(0),A} &= i\sqrt{\pi}.
\end{aligned} \tag{16}$$

The integrals in the B-parts are directly well convergent. Their calculation is a bit more difficult, but after a number of transformations all can be taken into a form to be found in tables. The results are

$$\begin{aligned}
\Pi_2^{(0),B} &= 4\sqrt{\pi} + \frac{(3 - 3\sqrt{2} - 8\pi + 2\sqrt{2}\pi) \zeta(\frac{3}{2})}{2\sqrt{\pi}}, \\
\Pi_3^{(0),B} &= 5\sqrt{\pi} + \frac{(6 - 6\sqrt{2} - 4\pi + 2\sqrt{2}\pi) \zeta(\frac{3}{2})}{2\sqrt{\pi}}, \\
\Pi_5^{(0),B} &= \frac{1}{2}\sqrt{\pi} \left( 2 + (-4 + \sqrt{2}) \zeta(\frac{3}{2}) \right).
\end{aligned} \tag{17}$$

Together with the A-parts we get finally

$$\begin{aligned}
\Pi_2^{(0)} &= \frac{g^2}{(4\pi)^{3/2}} \frac{T}{\sqrt{gB}} \left[ 4(1+i)\sqrt{\pi} + \frac{(3 - 3\sqrt{2} - 8\pi + 2\sqrt{2}\pi) \zeta(\frac{3}{2})}{2\sqrt{\pi}} \right], \\
\Pi_3^{(0)} &= \frac{g^2}{(4\pi)^{3/2}} \frac{T}{\sqrt{gB}} \left[ 5(1+i)\sqrt{\pi} + \frac{(6 - 6\sqrt{2} - 4\pi + 2\sqrt{2}\pi) \zeta(\frac{3}{2})}{2\sqrt{\pi}} \right], \\
\Pi_5^{(0)} &= \frac{g^2}{(4\pi)^{3/2}} \frac{T}{\sqrt{gB}} \left[ i\sqrt{\pi} + \frac{1}{2}\sqrt{\pi} \left( 2 + (-4 + \sqrt{2}) \zeta(\frac{3}{2}) \right) \right].
\end{aligned} \tag{18}$$

The corresponding numerical values,

$$\begin{aligned}
\Pi_2^{(0)} &= \frac{g^2}{(4\pi)^{3/2}} \frac{T}{\sqrt{gB}} (-5.80 + 7.09i), \\
\Pi_3^{(0)} &= \frac{g^2}{(4\pi)^{3/2}} \frac{T}{\sqrt{gB}} (1.04 - 8.9i), \\
\Pi_5^{(0)} &= \frac{g^2}{(4\pi)^{3/2}} \frac{T}{\sqrt{gB}} (-4.21 + 1.8i)
\end{aligned} \tag{19}$$

were obtained already in [10] (however, with a wrong sign of the imaginary parts). The above expressions have to be used in Eq.(10) to obtain final result. The sum of  $\Pi_3 + \Pi_5$  equals,  $\Pi_3 + \Pi_5 = [-3.17 - 7.09i]$ . The imaginary part is signaling the instability of the state because of the tachyon mode, and the real one is responsible for the screening of transverse gluon fields. The real and imaginary parts are of the same order of magnitude. This is similar to the case of Landau's damping at finite temperature.

Let us turn to the real part and substitute it in the Schwinger-Dyson equation

$$D^{-1}(k^2) = k^2 - \Pi(k) \quad (20)$$

for the neutral gluon Green function. We obtain for the mean values

$$\begin{aligned} \langle s = 1 | D^{-1}(h^2) | s = 1 \rangle &= h^2 - \text{Re}(\Pi_2) h^2 \\ &= h^2 \left( 1 + 5.8 \frac{T}{\sqrt{gB}} \right) \end{aligned} \quad (21)$$

and

$$\begin{aligned} \langle s = 2 | D^{-1}(h^2) | s = 2 \rangle &= h^2 - \text{Re}(\Pi_3 + \Pi_5) h^2 \\ &= h^2 \left( 1 + 7.09 \frac{T}{\sqrt{gB}} \right). \end{aligned} \quad (22)$$

These are the expressions of interest.

Two important conclusions follow from Eqs.(21),(22). First, for the transverse modes in the field presence, there is no fictitious pole similar to that of in the one-loop approximation for zero external field background at finite temperature [15]. The external field acts as some kind resummation removing this singularity. Second, there is no magnetic screening mass in one-loop order. The transverse components of the gluon field remain long range in this approximation, as at zero external field [15].

Possible resolutions of the zero one-loop magnetic mass are obvious: 1) the mass is generated in some kind resummation of perturbation series (as this is well known at zero external field case); 2) there are no magnetic mass for neutral gluons as in the case of usual magnetic fields. The problem requires nonperturbation methods of computation.

### 3 Magnetic mass on a lattice

To solve the problem formulated in the end of the previous section, we calculate the magnetic mass of the Abelian chromomagnetic field by using Monte-Carlo (MC) simulations on a lattice. For this purpose we, following Ref.[19], investigate the behavior of the average magnetic flux penetrating a lattice plaquette oriented

perpendicular to the magnetic field direction. To introduce the classical magnetic field (3) on a lattice we apply the twisted boundary conditions discussed below.

In the MC simulations, we use the hypercubic lattice  $L_t \times L_s^3$  with hypertorus geometry. The standard Wilson action of the  $SU(2)$  lattice gauge theory is

$$S_W = \beta \sum_x \sum_{\mu < \nu} \left[ 1 - \frac{1}{2} \text{Tr} \left[ \mathbf{U}_\mu(x) \mathbf{U}_\nu(x + a\hat{\mu}) \mathbf{U}_\mu^\dagger(x + a\hat{\nu}) \mathbf{U}_\nu^\dagger(x) \right] \right], \quad (23)$$

where  $\beta = 4/g^2$  is the lattice coupling constant,  $g$  is a bare gauge coupling,  $\mathbf{U}_\mu(x)$  is the link variable located on the link leaving the lattice site  $x$  in the  $\mu$ -th direction. The link variables  $\mathbf{U}_\mu(x)$  are  $SU(2)$  matrices decomposed in terms of the unity,  $I$ , and Pauli  $\sigma_j$ , matrices in color space,

$$U_\mu(x) = IU_\mu^0(x) + i\sigma_j U_\mu^j(x) = \begin{pmatrix} U_\mu^0(x) + iU_\mu^3(x) & U_\mu^2(x) + iU_\mu^1(x) \\ -U_\mu^2(x) + iU_\mu^1(x) & U_\mu^0(x) - iU_\mu^3(x) \end{pmatrix}. \quad (24)$$

Next let us incorporate the external Abelian magnetic field (3) into this formalism. As in Refs.[6], [18] we represent the field in terms of external fluxes  $\varphi$ . The constant homogeneous external flux  $\varphi$  in the third spatial direction can be introduced by applying the following twisted boundary conditions (t.b.c.) [18]:

$$\begin{aligned} U_\mu(L_t, x_1, x_2, x_3) &= U_\mu(0, x_1, x_2, x_3), \\ U_\mu(x_0, L_s, x_2, x_3) &= U_\mu(x_0, 0, x_2, x_3), \\ U_\mu(x_0, x_1, L_s, x_3) &= e^{i\varphi} U_\mu(x_0, x_1, 0, x_3), \\ U_\mu(x_0, x_1, x_2, L_s) &= U_\mu(x_0, x_1, x_2, 0). \end{aligned} \quad (25)$$

These give

$$\begin{aligned} U_\mu^0(x) &= \begin{cases} U_\mu^0(x) \cos(\varphi) - U_\mu^3(x) \sin(\varphi) & \text{for } x = (x_0, x_1, L_s, x_3) \text{ and } \mu = 2 \\ U_\mu^0(x) & \text{for other links} \end{cases}, \\ U_\mu^3(x) &= \begin{cases} U_\mu^0(x) \sin(\varphi) + U_\mu^3(x) \cos(\varphi) & \text{for } x = (x_0, x_1, L_s, x_3) \text{ and } \mu = 2 \\ U_\mu^0(x) & \text{for other links} \end{cases}. \end{aligned}$$

The edge links in all directions are identified as usual periodic boundary conditions except for the links in the second spatial direction for which the additional phase  $\varphi$  is added (Fig. 1). In the continuum limit, such t.b.c. settle the magnetic field with the potential  $\bar{A}_\mu = (0, 0, Bx^1, 0)$  (3). The magnetic flux  $\varphi$  is measured in angular units and can take continuous values from 0 to  $2\pi$ .

More details on the t.b.c. can be found in Ref.[19]. In this paper, the twist of the boundary conditions was applied to introduce the magnetic flux of the Dirac monopole. Then the magnetic mass of this non-Abelian magnetic field is measured by investigating the average plaquette values for the twisted and



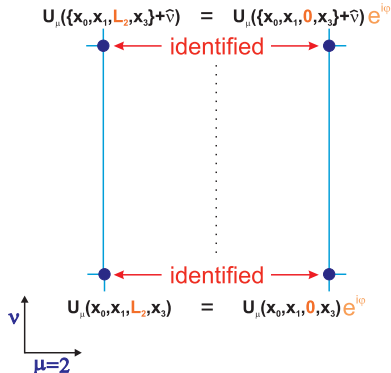


**Figure 1:** The plaquette presentation of the twisted boundary conditions.

untwisted lattices. The main object of such type investigations is the difference (magnetic flux through a lattice plaquette perpendicular to the  $OZ$  axis):

$$\langle U_{untwisted} \rangle - \langle U_{twisted} \rangle = f(m, L_s), \quad (26)$$

which is fitted for each lattice geometry  $L_t \times L_s^3$  by different functions  $f(m, L_s)$ . Below we follow this approach and measure the magnetic mass of the Abelian field of interest. The temperature is introduced in a standard way through a lattice asymmetry in the temporal direction ( $L_t < L_s$ ). The measurements were fulfilled for the value of  $\beta = 2.6$  in the perturbation regime for the deconfinement phase. Lattices with  $L_t = 4$  and  $L_s$  up to 32 were used. To update the lattice, heat-bath algorithm with overrelaxation was used [21]. To thermalize the system, up to 6000 MC iterations were used. The plaquette average is calculated by averaging up to 10000 working iterations.

To estimate the behavior of magnetic fields a large amount of simulation data must be prepared. Unfortunately, traditional computational resources are lack to perform the detailed analysis. In our case, we use the General Purpose computation on Graphics Processing Units (GPGPU) technology allowing to study large lattices on personal computers. GPU programming model implemented here and some technical details on MC simulations on ATI graphics processing units (GPU) are given in Ref. [16].

For GPU simulations, we apply GPU cluster of AMD/ATI Radeon GPUs: HD4850, HD4870, HD5850 and HD5870. A peak performance of the GPU cluster used is up to 8 Tflops. The common checkerboard scheme is used for internal GPU parallelization. Simple parallelization scheme is implemented on the cluster level – each node in the cluster performed independent MC simulation for parameters given by the host system. Simulated data set is collected after each MC run by the host system, as the host system we use one of cluster nodes. Such scheme allows to increase linearly the performance of cluster with increasing the number of nodes in the cluster.

To design the GPU-applications it must be accounted for that each general-purpose register (GPR) and memory cell has the four 32-bit components (single

precision) called GPR-slots and usually designated as .x, .y, .z and .w. Thus, for  $SU(2)$  model it is natural to store all the components of link matrices ( $U_\mu^0(x)$ ,  $U_\mu^1(x)$ ,  $U_\mu^2(x)$  and  $U_\mu^3(x)$ ) (see Eq.(24)) as one GPU-cell. For example, if GPR  $R1 = \mathbf{U}_\mu(x)$ , then the components of this register are  $R1.x = U_\mu^0(x)$ ,  $R1.y = U_\mu^1(x)$ ,  $R1.z = U_\mu^2(x)$  and  $R1.w = U_\mu^3(x)$ . So, lattice data are stored with the single precision, MC updating is performed with the single precision whereas all averaging measurements were performed with the double precision to avoid error accumulation.

Distinguishing feature of the employed program model is that all data necessary for simulations are stored in GPU memory. GPU carries out intermediate actions and returns the results to the host program for final data handling and output. We avoid any data transfer during the run-time between the host program and kernels to speed-up the execution process.

To generate the pseudo-random numbers for MC procedure, three different pseudo-random number generators are used: RANMAR, RANLUX and XOR128 [17]. The last one allows to obtain the maximal performance but is not widely used in MC simulations. So, all the results were checked with the slower generators RANMAR and RANLUX.

Performance analysis indicates that the GPU-based MC simulation program shows better speed-up factors for big lattices in comparing with the CPU-based one. For the majority lattice geometries the GPU vs. CPU (single-thread CPU execution) speed-up factor is above 50x and for some lattice sizes could overcome the factor 100x.

Thus, GPU-based MC program allows to calculate the difference (26) for a wide interval of lattice geometries. Also, up to 1000 independent runs for each lattice size were performed in order to decrease the dispersion of the obtained values  $f(m, L_s)$ . The whole set of simulation data for different lattice geometries was fitted with the several functions which correspond to the different behavior of magnetic flux.

The flux value  $f(m, L_s)$  is determined by (26) and shown in Table 1 and Figure 2. The whole set of the data obtained in MC simulations is divided into 15 bins. The mean values are presented as the black points and the corresponding  $2\sigma$  confidential level intervals are depicted by the vertical lines. The plotted data refer to  $L_t = 4$  and  $\beta = 2.6$ . The relative errors decrease from 11.1% to 4.1% with increasing  $L_s$ , as it should be.

In order to investigate different hypothesis for the behavior of the magnetic flux we try to fit the MC data with some set of functions by means of the  $\chi^2$ -method. The first test function  $C/r^2$  corresponds to the magnetic flux tube formation. Here  $r$  is the lattice size  $L_s$  in the  $X$  and  $Y$  directions,  $C$  is an unknown parameter. The total magnetic flux through the lattice is conserved in this case. Next function  $C/r^4$  describes the Coulomb-like behavior and the function  $C/r^2 \exp(-m^2 r^2)$  is signaling the generation of the magnetic mass  $m$  [19]. The last functions  $C/r \exp(-mr)$  and  $C/r$  can be related to increasing of

the field strength with a temperature growth. This is because the total magnetic flux through the lattice is growing faster than in the case of the magnetic flux tube formation.

The fitted curves are shown in Figure 2. These are: a) the visually coinciding solid curves –  $C/r$ ,  $C/r \exp(-mr)$ ,  $C/r \exp(-mr^2)$ ; b) the dot curve –  $C \exp(-mr^2)$ ; c) the dash curve –  $C/r^2$ ; d) the dash-dot curve –  $C/r^4$ .

The numerical results of fitting procedure are collected in Table 2. The table contains the test functions, the values of the  $\chi^2$ -function corresponding to the 95% confidence level, the obtained magnetic masses  $m$  and parameters  $C$ .

As it follows from Table 2, the best fit function is  $C/r \exp(-mr)$  with a small value of the magnetic mass  $m = 1.25 \times 10^{-6}$ . The value of  $\chi^2$  function in this case is very close to the  $m = 0$  situation and statistically these cases are indistinguishable. Really, the statistical errors are larger than the fitted value of  $m$ . Thus, from the performed analysis we can conclude that the neutral component of the gluon field is not screened at high temperature like usual magnetic field. This result is in agreement with that of previous section.

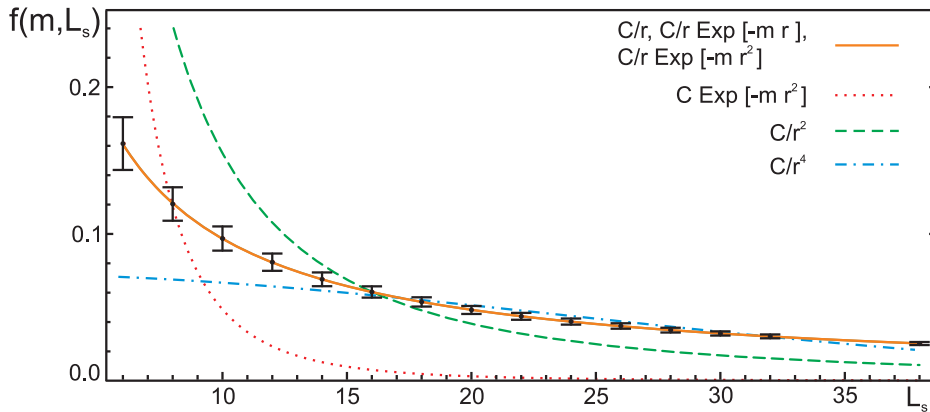


**Figure 2:**  $f(m, L_s)$  versus  $L_s$  and fitting curves ( $L_t = 4$ ,  $\beta = 2.6$ ).

$f(m, L_S)$	$L_S$
$0.161 \pm 0.018$	6
$0.12 \pm 0.011$	8
$0.097 \pm 0.008$	10
$0.081 \pm 0.006$	12
$0.069 \pm 0.005$	14
$0.06 \pm 0.004$	16
$0.054 \pm 0.003$	18
$0.048 \pm 0.003$	20
$0.044 \pm 0.002$	22
$0.04 \pm 0.002$	24
$0.037 \pm 0.002$	26
$0.0345 \pm 0.0016$	28
$0.0322 \pm 0.0014$	30
$0.0302 \pm 0.0013$	32
$0.025 \pm 0.001$	38

**Table 1:**  
Monte-Carlo data.

Fit function	Abelian field		
	$\chi^2$	$C$	$m$
$C \exp(-mr)$	901.8	0.063	$m = (2.44^{+0.06}_{-0.06}) \times 10^{-2}$
$C \exp(-m^2 r^2)$	1924.4	0.035	$m = (1.57^{+0.02}_{-0.02}) \times 10^{-2}$
$C/r$	7.090	0.911	
$C/r \exp(-mr)$	7.086	0.912	$m = (1.25^{+52}_{-54}) \times 10^{-6}$
$C/r \exp(-m^2 r^2)$	7.090	0.911	$m^2 = (2.4^{+5951.2}_{-5784}) \times 10^{-10}$
$C/r^2$	31400	28.13	
$C/r^2 \exp(-m^2 r^2)$	7550	18.26	$m^2 = -3.3 \times 10^{-5}$
$C/r^4$	159500	248.9	
$C/r^4 \exp(-m^4 r^4)$	161000	10.0	$m = 0.0$

**Table 2:** Fit results for magnetic mass of Abelian magnetic field.

The result obtained is unexpected one. In fact, we assumed to find a nonzero value of the order  $m_{magn.} \sim g^2 T$ , as at zero external field [19]. To be sure in our analysis, we have reproduced the later result as well. It should also be noted that due to a huge amount of data we have guaranteed that the absolute value of errors is of  $10^2 - 10^3$  times less than the value of the corresponding quantity.

## 4 Discussion

We performed calculation of the magnetic mass for neutral gluons in the Abelian chromomagnetic field at high temperature. Such type fields have to be spontaneously generated in deconfinement phase. They are stable due to large value of the charged gluon magnetic mass [4], [18]. The results obtained in continuum field theory coincide with that of MC simulations on a lattice. In both cases zero value is determined with the accuracy proper to the methods used. Hence, we conclude that such magnetic fields are long range ones. This, in particular, means that Abelian magnetic fields, being the solutions to the non-Abelian gauge field equations without sources, are spontaneously created at high temperature and exist till the confinement phase transition happens. This also concerns the electroweak sector of the standard model. In this case only the non-Abelian constituent of the magnetic field related to the  $SU(2)$  weak isospin group is spontaneously created at high temperature. The constituent related to the weak hypercharge subgroup  $U(1)_Y$  is zero.

Interesting additional arguments in favor of spontaneous vacuum magnetization at high temperature were obtained in sect. 3. In the measurements fulfilled, we observed that for the fitting function  $f(m, L_s) = C/r^2$  corresponding to the

magnetic flux tube formation the  $\chi^2$  value is very large and entirely inconsistent with the data. But in the geometry of measurements it describes the conservation of the magnetic flux introduced by the twist of the boundary conditions. The best fit functions  $C/r$ ,  $C/r \exp(-mr)$  with very small (actually, zero)  $m$  are signaling an increase of the mean magnetic field strength penetrating the plaquette perpendicular to the field direction. As a result, the flux through the whole  $(X - Y)$  plane should increase. The only natural explanation is the spontaneous generation of the field inside the volume of the lattice.

Since the field created at high temperature is described by the solution Eq.(3) which spoils gauge invariance, the question of its physical content arises. One of the possible ways to restore gauge invariance consists in formation of the domain structure having a special boundary which ensures the invariance. Other possibility consists in spontaneous breaking of color symmetry at high temperatures having macroscopic consequences and some remnants at low temperatures after the confinement phase transition (the electroweak phase transition) happens. These alternatives as well as other scenarios require separate investigations.

As a general conclusion we note that the presence of Abelian temperature dependent magnetic fields in high temperature phase of QCD and other gauge field theories has to be taken into consideration when various phenomena are investigated.

## 5 Acknowledgements

One of us (VS) was supported by DFG under Grant No BO1112/16-1. He also thanks the Institute for Theoretical Physics of Leipzig University for kind hospitality.

## References

- [1] P. Cea, L. Cosmai and M. D’Elia, JHEP **0712**, 097 (2007).
- [2] A. O. Starinets, A. S. Vshivtsev and V. C. Zhukovsky, Phys. Lett. B **322**, 403 (1994).
- [3] K. Enqvist and P. Olesen, Phys. Lett. B **329**, 195 (1994) [arXiv:hep-ph/9402295].
- [4] V. Skalozub and M. Bordag, Nucl. Phys. B **576**, 430 (2000) [arXiv:hep-ph/9905302].
- [5] V. V. Skalozub, Int. J. Mod. Phys. A **11**, 5643 (1996).
- [6] V. I. Demchik and V. V. Skalozub, Phys. Atom. Nucl. **71**, 180 (2008).

- [7] G. K. Savvidy, Phys. Lett. B **71**, 133 (1977).
- [8] D. Ebert, V. C. Zhukovsky and A. S. Vshivtsev, Int. J. Mod. Phys. A **13**, 1723 (1998).
- [9] V.V. Skalozub and A.V. Strelchenko, Eur. Phys. J. C **33**, 105 (2004).
- [10] M. Bordag and V. Skalozub, Phys. Rev. D **75**, 125003 (2007) [arXiv:hep-th/0611256].
- [11] M. Bordag and V. Skalozub, Phys. Rev. D **77**, 105013 (2008) [arXiv:0801.2306 [hep-th]].
- [12] J. S. Schwinger, Phys. Rev. D **7**, 1696 (1973).
- [13] M. Bordag and V. Skalozub, Eur. Phys. J. C **45**, 159 (2006) [arXiv:hep-th/0507141].
- [14] W. Y. Tsai and A. Yildiz, Phys. Rev. D **8**, 3446 (1973) [Erratum-ibid. D **9**, 2489 (1974)].
- [15] O. K. Kalashnikov, Fortsch. Phys. **32**, 525 (1984).
- [16] V. Demchik and A. Strelchenko, arXiv:0903.3053 [hep-lat].
- [17] V. Demchik, Comp. Phys. Comm. **182**, 692 (2011), doi: 10.1016/j.cpc.2010.12.008; arXiv:1003.1898 [hep-lat].
- [18] V. Demchik and V. Skalozub, arXiv:hep-lat/0601035.
- [19] T. A. DeGrand and D. Toussaint, Phys. Rev. D **25** (1982) 526. Phys. Rev. D **25** (1982) 526.
- [20] G. 't Hooft, Nucl. Phys. B **153**, 141 (1979).
- [21] M. Creutz, Phys. Rev. D **36** (1987) 515.